JA

Simultaneous Soft X-ray and GeV Gamma-Ray Observations of BL Lac Object AO 0235+164

G. Madejski, T. Takahashi, M. Tashiro, H. Kubo,
R. Hartman, T. Kallman, and M. Sikora

SW9615

LABORATORY FOR HIGH ENERGY
ASTROPHYSICS

National Aeronautics And Space Administration
Goddard Space Flight Center
Greenbelt, Maryland 20771

X-RAY: 95-18

SIMULTANEOUS SOFT X-RAY and GeV GAMMA-RAY OBSERVATIONS OF BL LAC OBJECT AO 0235+164

G. Madejski[1,2], T. Takahashi[3,4], M. Tashior[3], H. Kubo[3],
R. Hartman[1], T. Kallman[1], and M. Sikora[1,5,6]

Code 666
X-ray Astrophysics Branch
Laboratory for High Energy Astrophysics
NASA/Goddard Space Flight Center
Greenbelt, Maryland 20771

Accepted for publication in The Astrophysical Journal (Jan. 20, 1996)

[1] Laboratory for High Energy Astrophysics, NASA/GSFC
[2]Universities Space Research Association
[3]Physics Dept., U. of Tokyo
[4]ISAS, Sagamihara
[5]Copernicus Center, Warsaw
[6]JILA/U. of Colorado

Simultaneous Soft X–ray and GeV Gamma–ray Observations of BL Lac Object AO 0235+164

Greg Madejski[1,2], Tadayuki Takahashi[3,4], Makoto Tashiro[3], Hidetoshi Kubo[3],
Robert Hartman[1], Timothy Kallman[1], and Marek Sikora[5,1,6]

[1]Lab for High Energy Astrophysics, Code 666, NASA/Goddard Space Flight Center, Greenbelt, MD 20771
[2]With Universities Space Research Association
[3]Physics Dept., Univ. of Tokyo, 7-3-1, Hongo, Bunkyo-ku, Tokyo 113, Japan
[4] Institute of Space and Astronautical Science, 3-1-1 Yoshinodai, Sagamihara, Kanagawa, 299, Japan
[5]Copernicus Center, ul. Bartycka 18, 00-716, Warsaw, Poland
[6]JILA/University of Colorado, Boulder, CO

ABSTRACT

We present data collected during a simultaneous GeV γ–ray (CGRO Egret) and X–ray (Asca) observation of BL Lac object AO 0235+164 ($z = 0.94$); we also present ROSAT PSPC X–ray data, obtained 6 months earlier. The X–ray spectra from both ROSAT and Asca confirm a substantial photoelectric absorption beyond the value expected due to our Galaxy, which is most likely due to heavy elements in the ISM of an intervening galaxy at $z = 0.524$; it is possible to measure the elemental abundances in it *modulo* the hydrogen spin temperature T_S. By comparing the absorption in our data to the 21 cm absorption, we can limit T_S to at most ~ 700 K.

The ROSAT data imply a rapid ($\sim$ 3-day) doubling of the soft X–ray flux, and a subsequent quasi-exponential decay, whereas no variability is apparent in the Asca or Egret data. We detect a significant spectral change of the BL Lac X–ray continuum between the ROSAT and Asca observations; Asca data show that the spectrum is substantially harder (with the energy power law index $\alpha \sim 1$ *vs.* ~ 2) and fainter than in the ROSAT data. The simplest interpretation of this spectral variability is that the ROSAT data are dominated by a bright, soft tail of a synchrotron component, which disappeared during the Asca observation, uncovering a harder Compton component.

The Egret data imply a lower GeV flux than in the previous observations, with no apparent change of the GeV spectrum. The ratio of the γ–ray – to the X–ray flux (in $E \times F(E)$) for this radio-discovered object is roughly 30, which is very substantially higher than that inferred for X–ray – discovered BL Lacs, suggesting an important difference in the structure between the two sub-classes of BL Lac objects.

1. Introduction

AO 0235+164, one of the "original" BL Lac objects, was discovered on the basis of the optical ID of a variable radio source by Spinrad and Smith (1975); its redshift (inferred from weak emission lines) is 0.94 (Cohen et al. 1987). It is one of the most optically variable BL Lacs, varying by a factor of 100 (Rieke et al. 1976). Importantly, Compton Gamma–ray Observatory Egret data show strong GeV γ–ray emission (Hunter et al. 1993), with a flux variable from observation to observation (von Montigny et al. 1995); no rapid (time scale less than $\sim$ a week) GeV variability has been reported, but this may be due to sparse sampling. AO 0235+164 has all the characteristics of Optically Violent Variable quasars (including the GeV emission), except that it shows only very weak optical emission lines, and as such, it may be an intermediate object between the two sub-classes of a larger class called "blazars" – true, lineless BL Lacs, and OVVs.

High resolution optical spectroscopy revealed two absorption line systems, one at $z_{ab1} = 0.524$, and a

weaker one at $z_{ab2} = 0.852$ (Burbidge et al. 1976; Rieke et al. 1976). The system at $z_{ab1} = 0.524$ is also observed in 21 cm absorption (Roberts et al. 1976; Wolfe and Wills 1977). Historically, the absorption data added to the body of evidence for the extragalactic nature of BL Lac objects, and by extension, radio-loud quasars. It was speculated that the location of this object behind a galaxy could explain the variability as a result of gravitational microlensing (Ostriker and Vietri 1985), although this has been disputed recently (Abraham et al. 1993; see also Wolfe, Davis and Briggs 1982). Nonetheless, the column density of the absorbing material, as inferred from the ground-based observations, should be sufficient – under reasonable Cosmic abundances – to show up as photoelectric absorption in the X–rays. Indeed, the previous data (from the Einstein Observatory Imaging Proportional Counter, or the IPC) showed such absorption, at a level significantly greater than expected from our own Galaxy (Madejski 1994). Since the IUE UV data (Snijders et al. 1982) imply that the hydrogen column density in that system at $z_{ab2} = 0.852$ is at most 10^{17} cm^{-2}, several orders of magnitude lower than the $z_{ab1} = 0.524$ system, we can safely assume that such absorption is entirely dominated by the latter; this is further supported by a non-detection of the 21 cm absorption redshifted to $z = 0.852$. With the optical and radio data available, the X–ray absorption should yield elemental abundances in the intervening galaxy, although it is important to note that the $z = 0.524$ system is unusual in its own right, showing strong emission lines *without* a bright nuclear source, and may not be representative of ordinary galaxies (Cohen et al. 1987).

The goal of the observations reported here was therefore two-fold: one was to precisely measure the soft X–ray spectrum, in order to study the details of the photoelectric absorption of the intervening system. The other was to obtain the X–ray and γ–ray data *simultaneously*, to determine the relationship of the X–ray spectrum to the GeV spectrum, which is important for modelling of the overall electromagnetic emission from this highly variable object. We note here that the source was a subject of a multi-wavelength ground-based campaign coincident with the GRO and Asca observations, but the results from other wavelengths will be reported elsewhere. We present the ROSAT, Asca and Egret data in Section 2, show the spectral fits in Section 3, and discuss the X–ray absorption and overall X–ray – to γ–ray spectrum in Section 4.

2. Observations

2.1. ROSAT Observations

AO 0235+164 was observed 9 times by ROSAT PSPC between 21 July 1993 and 15 August 1993, roughly every 3 days, with each exposure lasting from $\sim$ 1200 to $\sim$ 4100 seconds. The log of the ROSAT observations is given in Table 1. The data were processed using SASS v. 6.4. The source was clearly detected in each exposure, with a position derived from the summed data at RA(2000.0) = $02^h38^m39.0^s$, dec(2000.0) = $16°37'05''$. This is within $10''$ of the radio position (RA(2000.0) = $02^h38^m38.4^s$, dec(2000.0) = $16°37'02''$), consistent with the ROSAT absolute pointing determination. No other sources brighter than 1/10 of the count rate of AO 0235+164 were detected in the image.

The PHA X–ray spectrum of the source was derived from the PSPC data in a standard manner, specifically by extracting counts from a circular region $3.75'$ in diameter, and the background counts from an annulus centered on the source, of inner diameter of $6.25'$ and outer diameter of $10'$, avoiding any obvious point sources. Only PSPC channels 12 through 211 were used, corresponding to a nominal energy range of 0.1 – 2.1 keV. For the spectral fitting, we binned the data using 5 original channels to a bin. The background-subtracted counting rates for each exposure are listed in Table 1.

It is clear from Table 1 that the source flux varied significantly from one exposure to another, with the highest count rate 4.7 times that of the lowest. The light curve of the source is shown in Figure 1a. The shape of the light curve is that of a rapid rise (which cannot be resolved with these data), and a more gradual

decay. To assure that the variability is not a result of instrumental effects, we measured the background count rate, normalized to a detection cell used for the source spectrum. This was relatively constant from one exposure to another, never reaching more than 12% of the source counting rate (cf. Table 1). We also examined individual exposures, and discovered no significant count rate variability within each exposure.

We examined the data to check if the variability is preferentially due to soft or hard photons within the ROSAT bandpass. To that end, we considered the photons below and above the nominal channel boundary of 1.0 keV, and plotted the ratio of soft to hard count rates in Figure 1b. While there is no obvious trend, the lowest flux point also corresponds to the hardest spectrum, but we do not consider this significant.

2.2. Asca Data

Asca observed AO 0235+164 four times, starting on February 4, 1994, with each exposure lasting $\sim$ 11,000 sec. The four observations (cf. Table 1) were spaced between 3 and 7 days apart, with the last exposure (Feb. 19, 1994) overlapping with the Egret observation. (The Asca exposures were designed to be fully overlapping with the Egret pointing, but this was precluded by an Egret target of opportunity.) Asca consists of four X-ray telescopes, with two having Gas Imaging Spectrometers (GIS2 and GIS3) and two having X-ray sensitive CCDs (known as SIS0 and SIS1) in the focal planes. All observations were performed in one-CCD mode, in the standard spectroscopy configuration. The data were selected using the fairly conservative screening criteria. These include: data were accepted when source was farther than 20° from the Earth limb during the orbit day, and farther than 5° (GIS) and 10° (SIS) during the orbit night; data were rejected within the South Atlantic Anomaly (SAA) and within 60 seconds of the crossing of the SAA boundary; data were rejected in the regions with geomagnetic rigidity < 6 GeV/c. The source was significantly detected in each exposure in all 4 detectors; the total "on source" time ranged from about 42 ksec to about 48 ksec. All data presented here were analyzed in the highest resolution "faint" mode, to assure that there would be no additional gain offset from the potential contamination by the scattered Sunlight; however, there was no discernible difference between the results of the "faint" and "bright" mode analyses.

The source counts were extracted from each image using a circular region of 6′ diameter for the SIS and 8′ diameter for the GIS data; we used somewhat smaller region than the standard values to minimize the contamination of this faint source counts by the background. The background was extracted from source-free regions of the same image as the source. For that, we used a region of the same area as the source region for the SISs, and 4 times greater area for the GISs. The resulting spectra from SIS0, SIS1, and GIS2 were then binned in groups of 2, 4, 8 or 16 original PHA channels to a bin, such that there would be at least ~ 20 counts per bin. Due to an on-board electronics malfunction in the GIS3 – where the two least significant bits of the analog-to-digital converter in the Pulse Height Discriminator circuit were stuck in a fixed pattern – all data for GIS3 needed to be binned with at least 8 channels to a bin. The background-subtracted counting rates are given in Table 1. In contrast to the ROSAT observation, there is no variability from one Asca exposure to another. We thus extracted a summed spectrum from the entire Asca observation.

2.3. Compton GRO Egret Observations

Egret observed AO 0235+164 starting on February 17, 1994. The total exposure lasted for 2 weeks. At $E > 100$ MeV, the source was detected at the level of 14×10^{-8} photons cm^{-2} s^{-1}, which is a 3 σ detection. This is significantly lower than measured by the original discovery observation (Hunter et al. 1993), and in fact was the lowest of all measurements of the source to date (von Montigny et al. 1995). Even though it was not possible to derive good limits on the source spectrum, in Figure 7 we plot the Egret data in the $E \times F(E)$ *vs.* E representation in 2 energy bands, 0.3 - 1 GeV, and 1 - 10 GeV, with the associated error bars on flux measurement. Even though in each of these bands the source was detected respectively only

at 2.2 and 2.7 σ, the purpose of plotting 2 separate energy channels in this Figure is to illustrate that the Egret data are consistent with a power law spectrum with $\alpha = 1.0$, reported by Hunter et al. (1993); such a spectrum would appear as a flat line in that Figure. With an assumed $\alpha = 1.0$, we infer a 1 GeV flux density (in $E \times F(E)$) of 0.014 keV cm^{-2} s^{-1}.

3. Spectral Fitting

3.1. ROSAT Spectrum

Since each ROSAT exposure did not produce enough source counts to yield a meaningful measurement of the spectrum, and there was no obvious change in the ratio of soft to hard count rates as a function of the source flux, we used summed ROSAT data in the subsequent spectral fitting; the mean background-subtracted counting rate was 0.17 cts s^{-1}. We fitted them to a simple, absorbed power-law model, using the cross-sections as given by Morrison and McCammon (1983) (hereafter MMC83). The fit is acceptable ($\chi^2 = 30.2/40$ PHA bins), with best-fit parameters $\alpha = 2.03^{+0.50}_{-0.45}$, and $N_{\rm H} = 3.0^{+0.8}_{-0.7} \times 10^{21}$ cm^{-2}; all spectral fits are tabulated in Table 2. (Throughout this paper, we use the energy power law index α, defined via flux density $F_E = F_o E^{-\alpha}$, and quote all errors as corresponding to 90% confidence contours for a single interesting parameter, i.e. $\chi^2 + 2.7$.) We show the data and corresponding residuals in Fig. 2. This value of the fitted column density is substantially larger than the Galactic value of 7.6×10^{20} cm^{-2} (determined using 21 cm data; Elvis, Lockman, and Wilkes 1989). As we argue in Sec. 4.1.1, the absorption above the Galactic value is likely to arise in the intervening galaxy at $z = 0.524$. We therefore also fit the data to a model consisting of a power law, a fixed absorbing column density of 7.6×10^{20} cm^{-2}, and additional MMC83 absorber at $z = 0.524$. (We note here that the use of the redshifted MMC83 absorber in this case is likely *not* to be appropriate, and we return to this point in Section 4.1.) The excess absorption is now $3.8^{+1.2}_{-1.1} \times 10^{21}$ cm^{-2}, and the power law index α is $1.67^{+0.32}_{-0.32}$, with $\chi^2 = 27.4/40$ PHA bins. Using either spectrum, the 0.5 – 2 keV flux ranges from 0.8 to 3.6 $\times 10^{-12}$ erg cm^{-2} s^{-1}, with a mean value of 1.7×10^{-12} erg cm^{-2} s^{-1}; the mean unabsorbed 1 keV flux density is 1.24 μJy.

3.2. Asca Spectrum

Since the source showed essentially no variability during the four Asca exposures, the Asca data from all 4 observations for each detector were summed and fitted in an analogous manner to the ROSAT data. We fitted data from all 4 detectors simultaneously, allowing each normalization to be free, to allow for residual calibration uncertainties. A simple, absorbed power law model (with all absorption at $z = 0$) yielded an acceptable fit (χ^2 of 341 for 354 PHA channels) with an index $\alpha = 1.01^{+0.09}_{-0.10}$, and column density of $2.7 \pm 0.5 \times 10^{21}$ cm^{-2}. The data and corresponding residuals for the GIS2 detector are shown in Fig. 3; other detector data look similar. Again, requiring that a fixed amount of absorption corresponding to 7.6×10^{20} cm^{-2} is due to our Galaxy, and allowing the excess absorption to be located at $z = 0.524$ – with the same *caveat* as in the previous section – we find that the excess is $4.6^{+1.3}_{-1.3} \times 10^{21}$ cm^{-2}, with the corresponding energy power law index $\alpha = 0.96 \pm 0.09$. Using either spectrum, the observed 0.5 – 2 keV flux is 0.4×10^{-12} erg cm^{-2} s^{-1}, with the unabsorbed 1 keV flux density of 0.3 μJy.

Even though we do not expect that an Fe K line would be detected from the BL Lac object, nonetheless we searched our data for limits on such a line, as it may be present in the intervening galaxy. Depending on the ionization stage of Fe, it would be expected at 4.2 - 4.7 keV at $z = 0.524$; a detection of such a line would be an indication that the intervening system is indeed an AGN with a strong X–ray emission, and that our X–ray spectrum of the BL Lac may be contaminated by a contribution from it. In order to determine a possible strength of such a line, we added a Gaussian line with an assumed width (σ) of 100 eV to the model with absorption at $z = 0.524$, and measured the resulting χ^2 as a function of the line energy in the interval

between 4 and 5 keV. We determined that no significant line is present there, with 90% confidence limit on the line equivalent width of ~ 60 eV. The limits on the line strength if emitted at $z = 0.94$ (and observed between 3 and 4 keV) are somewhat larger, ~ 100 eV.

3.3. Joint ROSAT – Asca Spectral Fits

A comparison of the ROSAT and Asca data clearly indicates that while the X–ray absorption is consistent between the two data sets, the power law index has significantly changed. That is best illustrated in Fig. 4, where on the same panel, we show the confidence contours for the ROSAT and Asca data. Quantitatively, the value of χ^2 for a fit to both data sets with the same power law and absorption (at $z = 0$), but free normalizations, is 431, *vs.* 371 if we allow separate power law indices for the two data sets (cf. Table 2). Could the difference in index be only related to the different bandpasses of ROSAT and Asca? Of course it is the low energy end of the combined spectrum that is sensitive to absorption, while the high end is sensitive to the underlying continuum. To test this, we restricted the Asca bandpass to extend only to 2 keV, and repeated the spectral fits (cf. Table 2). The spectral index is now $\alpha = 0.72^{+0.42}_{-0.43}$, well within 90% confidence regions of the full-bandpass Asca index, and significantly different than the ROSAT index. We thus conclude that the spectral variability is *not* just an artifact of the difference between the ROSAT and Asca bandpasses.

Is it possible that our assumed spectral form, an absorbed power law, is too simple of a shape to adequately describe the spectrum observed with the two satellites? Since the spectrum appears to be softer in the ROSAT observation, we investigated if the true spectral shape could be a hard power law with a "soft excess" of flux above the hard power law extrapolated to lower energies. To that end, we attempted a broken power law spectrum, described by one index $\alpha_{\rm lo}$ below some break energy E_b, and by another index $\alpha_{\rm hi}$ above E_b. First, we considered the ROSAT and Asca data separately. Individual fits to the ROSAT data yielded a marginal reduction of total value of χ^2 (with $\Delta\chi^2$ of 1.6 for the absorber at $z = 0$ and 1.1 for the absorber at $z = 0.524$, respectively), but with the addition of 2 free parameters, the χ^2/d.o.f. is actually worse. Similarly, we adopted such a broken power law model for the Asca data, which yielded $\Delta\chi^2$ of 1.0 for the absorber at $z = 0$ and 2.9 for the absorber at $z = 0.524$.

We also attempted a broken power law fit to the combined ROSAT and Asca data sets. As above, we adopted an absorbed broken power law model, where we required that the absorption (assumed at $z = 0$), the break energy E_b, and both power law indices $\alpha_{\rm lo}$ and $\alpha_{\rm hi}$ are the same for both data sets, but allowed the normalization to be free. The resulting total χ^2 is 428 for 394 PHA channels, vs. 371 if we adopt an absorbed power law model with separate power law indices for ROSAT and Asca data. We thus conclude that a broken power law model with a single set of parameters is *not* a better description of both ROSAT and Asca data than simple power laws with separate indices. The fact that the absorption between the two data sets is quite similar further strengthens the fact that both continua are well described by simple power laws; if this weren't the case, we would see a disagreement between the inferred values of $N_{\rm H}$ between the ROSAT and Asca data. We note here that other forms of the "soft excess" (thermal bremsstrahlung or a black body) yielded similar results.

Nonetheless, since the ROSAT data show steeper spectrum than the Asca data, the overall spectrum must have a "soft excess," but its contribution is strongly variable. Specifically, the break energy E_b, below which this "soft excess" dominates, must have shifted from somewhere *above* the ROSAT bandpass (> 2 keV) during the ROSAT observation to *below* the Asca bandpass (< 0.5 keV) during the Asca observation, such that the ROSAT data represent a nearly "pure" soft excess, while the Asca data are nearly a "pure" hard power law component. In fact, if the flux of the hard component were the same during the ROSAT

observation as we measured it in the Asca observation, we would have seen the break between the hard component and the "soft excess" at $\sim$ 5 keV. Unfortunately, this is of course beyond the bandpass of the ROSAT PSPC.

Using both data sets simultaneously, we can further constrain the amount of absorption and tighten the confidence ranges on the two spectral indices. For this, we fitted jointly the ROSAT and full-bandpass Asca data, allowing the index and normalization to be fitted independently, but requiring a common value of absorption for the two data sets. This procedure of course assumes that there was no change in absorption over 6 months, which is probably reasonable, given the confidence contours in Fig. 4. First, we adopted a simple absorbed power law model. The best-fit parameters for the joint ROSAT - Asca fit are : $N_{\rm H} = 2.8 \pm 0.4 \times 10^{21}$ cm^{-2}, $\alpha_{ROSAT} = 1.92^{+0.25}_{-0.27}$, and $\alpha_{Asca} = 1.02 \pm 0.08$, with $\chi^2 = 371$ for 394 PHA bins. Similarly to the individual ROSAT and Asca fits, we also attempted a model where we required that the excess absorption is as given by MMC83, at $z = 0.524$. This yielded $N_{\rm H}$ ($z = 0.524$) $= 4.2^{+0.9}_{-0.8} \times 10^{21}$ cm^{-2}, $\alpha_{ROSAT} = 1.77^{+0.25}_{-0.23}$, and $\alpha_{Asca} = 0.93^{+0.08}_{-0.07}$, with $\chi^2 = 368$ for 394 PHA bins (see Fig. 5). We note here that while there is an improvement in χ^2 of 3, this provides only a very marginal evidence that the excess absorber is at $z = 0.524$. We also note that the ROSAT and Asca data alone do not favor any particular redshift of the absorber ($\Delta\chi^2 < 2$ for any other redshift, as compared to $z = 0.524$).

4. Discussion

4.1. Excess Soft X–ray Absorption

4.1.1. Origin of the Excess Absorption

Both ROSAT and Asca data sets show that the X–ray data for AO 0235+164 can be fitted well by a model with a power law continuum and absorption, but the level of absorption exceeds that expected from the H I column measurements in our Galaxy. Of the various origins for this, we consider the following: first, it could be due to an excess in the ratio of X–ray column to H I in our own galaxy. This may be further divided into explanations due to absorption by gas which does not show up as 21 cm emission, or which is on a length scale not resolvable by 21 cm maps, or due to gas which is not hydrogen but which should be detectable in other ways. The other possibility we consider is that the gas is in the intervening galaxy.

The possibility that the excess absorber is, at least partially, in our Galaxy, in a form undetectable with the 21 cm technique may be supported by the case of the extragalactic source, NRAO 140, in which there is a substantial amount of molecular gas in the line of sight. In this object the molecular gas is measured in the ^{12}CO band (Bania, Marscher, and Barvainis 1991), and is contributing to X–ray absorption (Marscher 1988a; Turner et al. 1995). However, the galactic latitude of AO 0235+164 of $b = -39^{\circ}$ makes this less likely than for NRAO 140, at $b = -19^{\circ}$. The inspection of the ^{12}CO map in Dame et al. (1987) indicates no significant ^{12}CO emission at the location of AO 0235+164; however, the map resolution is modest. Under the premise that the diffuse Galactic 100 μm emission correlates well with the total (atomic and molecular) gas column density (Boulanger and Perault 1988), we also inspected the IRAS 100 μm map (Wheelock et al. 1994). We found that there is no significant ($> 20\%$ in intensity) structure within $30'$ of the position of AO 0235+164, and that the 100 μm surface brightness at the position of the source and its vicinity is $\sim$ 6.2 MJy/Sr. Using the conversion of Boulanger and Perault (1988) of 0.85 MJy/Sr per 1×10^{20} cm^{-2}, we obtain a value of 7.2×10^{20} cm^{-2}, in good agreement with the H I value, and thus the excess absorption is most likely extragalactic. We can probably discount the possibility that absorption is at or near $z = 0.94$, the redshift of the BL Lac itself, as no corresponding absorption features are present in the high-resolution optical spectrum (Cohen et al. 1987). Since, as we argued above, the IUE data rules out a significant neutral H column density of the system at $z = 0.852$, we conclude that the excess absorption in AO 0235+164 is

most likely due to the system at $z = 0.524$; this is further supported by the substantially stronger Mg II absorption at $z = 0.524$ than at $z = 0.852$ (see, e.g., Wolfe and Wills 1977).

The soft X–ray absorption observed in the ROSAT and Asca data is primarily due to helium, carbon and oxygen. In the previous fits, we used a redshifted Morrison and McCammon absorber, which assumes that the ratios of these elements to each other and to hydrogen are Solar, and thus the fit value, even though parametrized as an equivalent hydrogen column density, is a measure of the column density of He, C, and O *at ratios fixed to each other*. This, of course, is probably incorrect; the elemental abundances in the $z = 0.524$ system are unlikely to be Solar, and we discuss this below.

4.1.2. Elemental Abundances in the z = 0.524 System

The comparison of the optical and soft X–ray absorption against the 21 cm radio absorption in AO 0235+164 can, in principle, yield the measurement of elemental abundances relative to hydrogen in the intervening system. The use of the optical absorption lines is difficult, because only a study of ionized species is possible, and the relative population of ionized-to-neutral species is not well known. Also, these lines are extremely narrow, and thus are saturated, and it is necessary to revert to a curve-of-growth analysis. The X–ray route, which we attempt here, is more promising, but there are two important issues that have to be addressed: the first is the interpretation of the 21 cm measurements. There are no contemporaneous 21 cm and X–ray data, which adds to the uncertainty of such measurement if the absorption were variable, which is likely to be the case (cf. Wolfe et al. 1982). Furthermore, the determination of the 21 cm hydrogen column density in the intervening system is directly proportional to the hydrogen spin temperature T_S, which is poorly known. Nonetheless, there is at least a lower limit on T_S of 460 K (Briggs and Wolfe 1983), although Snijders et al. (1982), using the IUE UV data, argue that it is 140K. Roberts et al. (1976) give the 21 cm absorbing column density $N_{HI} \simeq 2.3 \times 10^{19} \times T_S$ cm^{-2}; with $T_S = 460$ K, $N_{HI} \simeq 10^{22}$ cm^{-2}.

The second issue arises from our inability to resolve the effects of absorption due to individual elements in our X–ray data via distinct absorption edges. In the fits presented in the previous sections, we made an assumption that the relative ratios of abundances of O to C to He in the $z = 0.524$ system are Solar. While it allows for a convenient parametrization of the absorption, this assumption is probably not valid, and this affects our conclusions. This is because a part of the excess absorption observed by us is due to helium. While C and O are certainly chemically processed in stars, He only partially originates from stars, but mainly from the Big Bang Nucleosynthesis. Olive and Steigman (1995) report that the generally accepted value of the ^{4}He mass fraction Y_p is between 0.22 and 0.24, corresponding to the ratio by number to hydrogen y_4^{BBN} of 0.072 to 0.08. The commonly accepted Solar value y_4^{Solar} is 0.1 (cf. MMC83), and thus the remainder, or the ratio (by number) of ^{4}He atoms produced by stellar and galactic chemical evolution to hydrogen atoms in the MMC83 absorber y_4^{Chem} is 0.024. This is very important in our study, since only 24% of He in the MMC83 absorber is "tied" to C and O via chemical evolution, and 76% is "tied" to hydrogen. As a result, instead of establishing the confidence limits on the absorption due to He, C, and O, we can only determine the limits on the processed elements *modulo* the combined column density of hydrogen and primordial helium. Of course we are making a (probably reasonable) assumption that the ratio of the *processed* He to O to C in the $z = 0.524$ system is Solar, but this is one assumption we can currently test only crudely (see Sec. 4.1.3).

We can measure such confidence limits by assuming that there are two separate absorbing columns in the $z = 0.524$ system: one "primordial", consisting of hydrogen plus 76% of He in the MMC83 absorber (which we denote as N_H^{BBN}), and the other "processed", consisting of no H, He at 24% of the MMC83 value, plus all heavier elements (which we denote as N_H^{Chem}); N_H^{Chem}, by design, has a Solar ratio of the chemically reprocessed elements heavier than He. We note that we assume that most of He (as well as other absorbing

elements) are not fully stripped, or else, they would have no X-ray opacity. We fitted simultaneously the ROSAT and Asca data to a power law model, with three absorbers: absorption due to our own Galaxy fixed at the 21 cm value, plus the two components of the $z = 0.524$ system as above, requiring that the absorption is common to the data from both instruments, but allow the power law spectral index to be fit independently (see Sec. 3.3). In Fig. 6a, we plot the confidence contours of the "primordial" vs. "processed" absorber, both parametrized as an equivalent hydrogen column density. As expected, the two parameters are correlated, but even at the unlikely zero value of the "processed" absorption, we cannot have more (at 90% confidence) than $N_{\rm H}^{\rm BBN}({\rm max}) \simeq 1.6 \times 10^{22}$ cm^{-2} of hydrogen absorption in the $z = 0.524$ system. This is very interesting, since via the constraint from the redshifted 21 cm data, we now can derive an upper limit on the spin temperature $T_{\rm S}$ in the $z = 0.524$ system to be less than ($N_{\rm H}^{\rm BBN}({\rm max})$ / $2.3 \times 10^{19}{\rm cm}^{-2}$) K, or $T_{\rm S} < 700$ K (cf. Figure 6a). We note that if all He is primordial (as it is sometimes assumed), the limit on $T_{\rm S}$ becomes even tighter, by about 15%. Finally, it is apparent from this Figure that we can establish the ratio of "processed" to "primordial" column densities A as a function of $T_{\rm S}$; A is is essentially the metallicity (as compared to Solar) in the intervening system. If $T_{\rm S} = 460$ K, then $A = 0.14 \pm 0.11$; if $T_{\rm S} = 140$ K, then $A = 1.3 \pm 0.3$.

4.1.3. Limits on Abundances of Individual Elements

In principle, given data with better energy resolution and S/N, we should be able to measure the depth of the C, O, Mg, and possibly Si K and Fe L edges (at their respective redshifted energies) separately, thus obtaining a direct measure of the column densities of these elements. C is redshifted out of the ROSAT bandpass; the modest energy resolution of ROSAT (where the O edge is) and limited statistics (where we could conceivably detect other edges) preclude such a measurement. The inspection of the data (cf. Figs 2 and 3) reveals no obvious discrete absorption or emission features in the spectrum of the source. In fact, as we discussed above, our data allow an absorber that is pure hydrogen and helium (cf. Fig. 6a). Nonetheless, we can place some confidence limits on the absorbing column densities for some elements. To that end, we performed spectral fits to the ROSAT and Asca data with a variable abundance absorber with only a given element present, placed at $z = 0.524$. As in the joint ROSAT + Asca fits discussed in Secs. 3.3 and 4.1.2, we fixed the Galactic absorption, and allowed the spectral indices to vary independently, but required the absorption to be the same for the two instruments. For O (and to a much lesser extent, for other elements) this is a "worst case" abundance limit, since an assumption that all the "processed" absorption is due to a single element requires larger columns that we really expect (compare Figs. 6a and 6b).

The effects of carbon cannot be distinguished from these of He, since its K edge is redshifted even out of the ROSAT bandpass. We thus first consider oxygen; we separated the absorbing effect of it from other elements by allowing two separate absorbing columns, parametrized as equivalent neutral hydrogen column density. One was pure oxygen at the Solar ratio of O to H, and the other was the "primordial" absorber as discussed above, containing H and 76% of the Solar fraction of He. Our results are shown in Fig. 6b, where we plot confidence contours of these absorbers. As expected, the two columns are anti-correlated, but importantly, we can limit the total equivalent hydrogen column of pure O absorber $N_{\rm H}^{\rm O} < 1 \times 10^{22}{\rm cm}^{-2}$, which corresponds to the a pure O column $N_{\rm O} < 7 \times 10^{18}{\rm cm}^{-2}$.

We performed similar fits for magnesium, iron (which are of particular interest, since the optical absorption lines in the $z = 0.524$ system are Mg II and Fe II), and silicon. The absorption from these heavier elements is not correlated with the "primordial" column, since their K edges are at higher energies than O, and thus Asca data would be able to resolve them. Our data can limit the columns of Si and Fe to $N_{\rm H}^{\rm Si} < 0.9 \times 10^{22}$ cm^{-2}, corresponding to $N_{\rm Si} < 3.4 \times 10^{17}$ cm^{-2} and $N_{\rm H}^{\rm Fe} < 2.7 \times 10^{22}{\rm cm}^{-2}$, corresponding to $N_{\rm Fe} < 9 \times 10^{17}{\rm cm}^{-2}$. For magnesium, there is a marginal evidence of an edge in the data, but this is

at less than 99% confidence; again, our limits for Mg are $N_{\rm H}^{\rm Mg} 2.4 \pm 2.0 \times 10^{22} {\rm cm}^{-2}$, corresponding to $N_{\rm Mg}$ of $\sim 9.6 \pm 8.0 \times 10^{17} {\rm cm}^{-2}$. We note that a high-resolution X–ray spectroscopic observations (as, e.g., with the X–ray Spectrometer planned to fly on Astro-E, or AXAF gratings), should yield the column densities of individual elements *directly* by resolving the individual edges.

4.1.4. Possible Variability of Absorption and its Implications

The level of soft X–ray absorption inferred from the ROSAT and Asca data is substantially lower than that measured in 1980 with the Einstein Observatory IPC, which corresponds to an excess (at $z = 0.524$) of $1.9^{+3.6}_{-1.4} \times 10^{22}$ cm^{-2} (Madejski 1994). This difference can be due to the residual calibration uncertainties of the IPC, but, given the variability of the redshifted 21 cm absorption by as much as a factor of 2 (Wolfe et al. 1982), there variability of the X–ray absorption is likely. Similar change in absorption, probably due to a passage of a molecular cloud in our own Galaxy through the line of sight, has been observed in the OVV quasar NRAO 140 (Marscher 1988b; Turner et al. 1995). In the IPC data for AO 0235+164, the errors on both the absorption and spectral index separately are large, but these fit parameters are correlated (see Figs 2 and 3 in Madejski 1994). The flux level of the object during the Einstein observation was comparable to the mean ROSAT flux, and thus the index in the IPC data was likely to be comparable to the ROSAT value. If this was the case, the errors in the IPC data are much smaller, and the difference in the excess absorption between the epochs of the IPC and the ROSAT/Asca observations must have been $\sim 10^{22}$ cm^{-2}.

While the evidence of the absorption variability is only tentative, it is worth considering the implications if it is real. In the reference to the variability of the 21 cm absorption, Wolfe et al. (1982) point out that either the source of the background radiation (in our case of X–rays) moved slightly, appearing from behind of a partially absorbing cloud, or the absorber moved across the line of sight to a steady source. With the superluminal expansion observed in many compact radio sources, the first possibility is not unlikely; even a tenth of a milliarcsecond of motion of an X–ray source would correspond to sampling a path shifted by $\sim$ a parsec at $z = 0.524$, which is certainly comparable to a size of molecular cloud structures. However, this would imply as-yet-unobserved change of the spatial structure of the X–ray emitting region. The other option is a transverse motion of an absorbing cloud across the line of sight in the intervening system. At $z = 0.524$, such a cloud would have to have a column density equal to the difference of the IPC and ROSAT/Asca columns, or $\sim 10^{22}$ cm^{-2}. A reasonable transverse velocity of such a cloud could be 200 km s^{-1} or less; the maximum distance travelled by such a cloud over $\sim$ 15 years would be then $\sim 2 \times 10^7$ cm/s $\times \sim 5 \times 10^8$ s $\simeq 10^{16}$ cm. Under the simplest symmetry assumptions, this would imply the density on the order of $\sim 10^6$ H atoms cm^{-3}, and total content of $\sim 4 \times 10^{54}$ H atoms, corresponding to $\sim 6 \times 10^{30}$ gram, which is not unreasonable; comparable structures within a galaxy are cores of molecular clouds, although the filling factor of such clouds is not large. Of course the X–ray absorption technique is not the only means to study such structures; high resolution absorption studies against AO 0235+164 or NRAO 140 in ^{12}CO could provide additional information.

Further refinement of the determination of the nature of the intervening absorber will be accomplished via future optical/UV spectroscopy. That is because both H Lyα and the H Lyman edge of the material in the $z = 0.524$ system are longward of the Galactic H Ly edge, and thus a careful determination of the $z = 0.524$ edge depth will provide the definitive answer as to the column density of hydrogen atoms. An HST observation of this object is already planned (R. Cohen, priv. comm.), but it is postponed until the object is brighter than the current level ($m_v \sim 19$). In addition to the measurement of discrete spectral features, such UV data will provide information as to the dust content of the intervening system, which is likely to be significant, judging by the steep IUE spectrum, with α of 3.5 ± 0.5 (Snijders et al. 1982) and red optical colors (Rieke et al. 1976). To that end, it would be particularly advantageous to obtain simultaneous X–ray

spectroscopy, allowing an extrapolation of the UV continuum to the energies beyond where it is affected by the Galactic (and the intervening) absorption; an additional benefit would be an ability to measure the gas – to – dust ratio in the intervening system.

4.2. X–ray Continuum

We observed AO 0235+164 in the X–ray band on two occasions: when it was bright, soft ($\alpha \sim 2$), and highly variable, and $\sim$ 6 months later, when it was fainter, harder ($\alpha \sim 1$), and relatively constant. This behavior of the X–ray continuum is almost exactly the opposite of what has been observed with Ginga in other BL Lac objects (cf. Tashiro 1992). In the case of PKS 2155-304, perhaps the most extensively observed BL Lac object in the X–ray band, the Ginga observation revealed that the spectrum hardened when the source got brighter, and then, in the course of becoming fainter, it also became steeper (Sembay et al. 1993). This happened on a relatively short time scale, on the order of several hours, but such behavior is also consistent with the variability observed at other epochs. This fits well into the synchrotron model for X–ray emission, where the spectrum steepens as a result of the decreasing lifetime of the radiating particles with increasing energy, as is expected in the case of synchrotron cooling. However, such a model also implies very low magnetic fields, and extreme Lorentz factors of the emitting electrons (Tashiro 1992; Tashiro et al. 1995). Alternatively, such a behavior can also be explained in terms of an inhomogeneous model without the necessity of involving extreme parameters of emitting regions. In such a model, the fastest and highest amplitude variability is produced by the innermost parts of a jet. Since in this model, the high energy cutoffs of synchrotron radiation spectra drop with distance (Ghisellini and Maraschi 1989), we can expect that soft X–rays – which form the high energy tail of the synchrotron component – arise from the innermost parts of a jet. At lower frequencies, the contribution from larger distances dominates, and variability time scale, if related to propagating disturbances or shocks, is correspondingly longer.

The spectral behavior of AO 0235+164 does not fit into such a pattern: instead, its continuum is hard when it is faint. This is in disagreement with a simple synchrotron model as the sole description of X–ray emission in all of our observations. We are driven to a conclusion that we observe two separate spectral components, where the drop in the intensity of the soft component uncovers the hard component. This interpretation, of course, makes a strong prediction, where in the intermediate flux states, the X–ray spectrum of this object is likely to show simultaneously both the hard component dominating the Asca data as well as a discernible "soft excess" of the component dominating the ROSAT data.

As to the origin of the soft ($\alpha \sim 2$) component of the X–ray emission, there is a circumstantial evidence that in AO 0235+164 we observe the high energy tail of the electron distribution radiating via the synchrotron process. As we mentioned above, this is most likely to be the case in PKS 2155-304. Further support is from the correlated optical, UV (IUE) and X–ray variability (Edelson et al. 1995; Brinkman et al. 1994), and for less-well studied objects, from the location of the X–ray spectrum on the extension of the UV power law (cf. Tashiro 1992; Madejski 1985).

What is the origin of the hard X–ray spectrum in AO 0235+164? The discovery of GeV γ–ray emission from the blazar 3C279 (Hartman et al. 1992), and subsequently from $\sim$ 40 other flat-spectrum compact extragalactic radio sources (see, e.g., Fichtel et al. 1994; von Montigny et al. 1995) established these objects as a class of GeV emitters, of which AO 0235+164 is a member. A plausible explanation of the mechanism responsible for the GeV emission in these sources is Comptonization, and the faint, hard X–ray emission could be the onset of the Compton component. It is interesting to note here that the interpretation of hard X–ray radiation as arising due to Comptonization fits well the *Ginga* observations of radio flat spectrum quasars, but not of BL Lac objects (Kii et al. 1992), at least not of the X–ray selected ones. There are

several classical, radio-selected BL Lac objects, where the relationship of the X–ray spectrum – which is hard, and *not* on the extrapolation of the optical – UV slope – suggests the Compton process as the origin of X–rays (see, e.g., another faint EGRET-detected BL Lac object PKS 0735+178, with $\alpha_x \sim 0.7$; Bregman et al. 1984, Madejski and Schwartz 1988). The Asca X–ray spectrum of AO 0235+164 appears similar to that of PKS 0735+178, and thus it is suggestive that the signature of the Compton emission in X–rays is more likely to be observed in the radio-selected BL Lacs.

A more detailed study of this putative Compton component may be aided by a comparison of our simultaneous X–ray – γ–ray data to that obtained in the 1993 campaign for the blazar 3C279 (Maraschi et al. 1994). It is likely that both objects were observed in their respective "low states", since in both cases, the levels of X–ray and γ–ray emission were amongst the lowest observed. For 3C279, the ratio of the 1 GeV to 1 keV flux per logarithmic frequency interval (in $E \times F(E)$) was roughly 8, whereas for AO 0235+164, we observe the ratio of ~ 30 (cf. Fig. 7). This is in contrast to the 1 GeV to 1 keV flux ratio of ~ 100 in the high state for 3C279; unfortunately, we do not have information about such ratio during high γ–ray state for AO 0235+164.

4.3. Overall electromagnetic emission

There is very good evidence that the overall electromagnetic emission in blazars is anisotropic, Doppler-boosted (beamed) toward the observer, and in reality, the monochromatic luminosity inferred under an assumption of isotropy must be reduced by a factor of $\delta^{-(k+\alpha)}$, where $k = 3$ is for a relativistically moving cloud of emitting gas, and $k = 2$ is for a steady-state jet, and α is the energy spectral index. (δ is defined in the standard way as $\Gamma^{-1}(1 - \beta\cos\phi)$, where Γ is the Lorentz factor of the jet, $\beta = v/c$, and ϕ is the angle to the line of sight.) In the radio regime, the evidence comes from superluminal expansion, observed with the VLBI. In the optical and UV, there is no irrefutable evidence for beaming, but the extremely rapid, large amplitude variability and high polarization would require extreme conditions without beaming (Blandford and Königl 1979). And finally, relativistic beaming is required in order to avoid absorption of GeV photons by X–ray photons in the pair production process (see, e.g., Maraschi, Ghisellini, and Celotti 1992).

Taking into account that absorption of γ–ray photons with energy E_γ is dominated by X–rays with energy E_x given by $E_\gamma(1+z)/\delta \times E_x(1+z)/\delta \sim (m_e c^2)^2$ (where E_γ and E_x are photon energies as measured by observer located at $\phi \leq 1/\Gamma$), the X–ray radiation field opacity for γ–rays at $E_\gamma \geq 1$ GeV for nonrelativistic jet ($\Gamma \sim 1$) is determined by compactness of radiation field in the soft X–ray band ($E_x \leq 1$ keV). Since for many blazars the X–ray compactness, as determined from the ratio of the X–ray luminosity variability magnitude to the variability time scale ($\Delta L_x/\Delta t$), gives optical thickness for pair production $\tau_{\gamma\gamma} \gg 1$, the observed transparency of the source for γ–rays up to GeV energies can be achieved only if $\delta \geq$ few. Assuming that the γ–rays and soft X–rays from AO 0235+164 are produced in the same region, we can calculate opacity for pair production from ROSAT data. Using formula given by eq. (3) in Mattox et al. (1993), but corrected for the error*, we find that for nonrelativistic outflow ($\Gamma \sim 1$) and the parameters observed in AO 0235+164 ($z = 0.94$, $\alpha = 2$, $T = 3$ days, and $F_{keV} = 2.5\mu$Jy), the opacity for 1 GeV photons would be $\tau_{\gamma\gamma} \sim 0.8 \times 10^4$, and $\delta > 3.1$ is required in order to have $\tau_{\gamma\gamma}(E_\gamma > 1 \text{ GeV}) < 1$.

---

* In the equation (3) in Mattox et al. (1993) the factor $(1 + z)$ should have power (2α), rather than $(4 + 2\alpha)$. The error is a consequence of using the wrong formula for the source frame differential luminosity. In an unnumbered equation three lines before equation (2), the factor $(1 + z)^3$ is correct only if followed by square of angular diameter distance which is $D_\phi = D_L/(1 + z)^2$. Therefore, in formulas (2) and (3) the factor $(1 + z)$ should have power (2α) and in eq. (4) the factor $(1 + z)$ should have power $-(2\alpha)$. The same error is followed in the paper by Montigny et al. (1995) in eqs. (5) and (6).

Strictly speaking, the above $\tau_{\gamma\gamma}$ argument for anisotropy only applies if the γ-ray emitting region is the same as the soft X–ray emitting region and, for now, we do not have any clear observational indications that this is the case. This is important, since the jets are likely to be inhomogeneous. However, since in some blazars the γ-ray variability is noted on time scales as short as a few days (Kniffen et al. 1993; von Montigny et al. 1995), and because γ–ray emission is accompanied by X–ray emission of the same population of relativistic particles, for such sources $\delta >$ a few can be deduced as well (note that X–rays produced in the γ–ray emission region can dominate the X–ray radiation field compactness locally, even if the observed X–rays are dominated by other jet regions).

While it is reasonably well established that the radio – through – UV (and in many cases, soft X–ray radiation) in blazars arises due to the synchrotron process in a jet or plasma clouds moving at relativistic speed, the location and the details of the mechanism responsible for the X–ray – to – γ–ray portion of the spectrum is still under some debate. The most common family of models invoked to explain the strong GeV emission in blazars involves Comptonization of lower energy photons, and it is likely that the faint, hard X–ray emission observed by us with Asca is the low energy end of the Compton component. In the two general classes of models, the seed photons for Comptonization are either produced by external radiation sources (the external radiation Compton, or ERC models), or internally due to the synchrotron process (the so-called synchrotron-self-Compton, or SSC models).

The ERC models rely either on the UV radiation from the central source, e.g. from the accretion disk around the central engine (Dermer, Schlickeiser, and Mastichiadis 1992), or radiation that is produced by scattering and reprocessing of the central radiation by emission line clouds and the intercloud medium (Blandford 1993; Sikora, Begelman, and Rees 1994). However, at least for the latter model, BL Lac objects are generally devoid of emission lines, and thus the scattering would have to happen on some hot ambient medium, existence of which cannot be proved directly by observations. The SSC models explain the γ–ray emission as resulting from Comptonization of synchrotron radiation, where both Compton and synchrotron radiation are produced by the same population of relativistic electrons/positrons accelerated locally within a relativistic jet (Rees 1967; Königl 1981; Marscher and Gear 1985; Ghisellini and Maraschi 1989).

Both the SSC and ERC models were recently invoked to describe the multi-wavelength data for the blazar 3C279 (Maraschi et al. 1994). One successful variant of the SSC model, capable of explaining the variability patterns in the radio, IR, optical, UV and X–ray bands, was proposed by Maraschi, Ghisellini, and Celotti (1992). In this model, the highest energy synchrotron photons, i.e., UV and in BL Lac objects soft X–rays, and the highest energy Compton photons, i.e. GeV γ–rays, are produced in the innermost parts of the jet. This the model predicts the largest variability of the Compton component in γ–rays, and the largest variability of the synchrotron radiation in UV or soft X–rays. The model seems to be in qualitative agreement with the multi-wavelength and multi-epoch observations of the blazar 3C279 (Maraschi et al. 1994). However, as was noted by these authors, the ERC model with variable Γ can fit these data as well.

The SSC interpretation of γ–ray production in AO 0235+164 may, at a first glance, be challenged by the fact that the fast variability in the soft X–ray band is not accompanied by variability in γ–rays. However, we can expect that synchrotron high energy tail, observed in soft X–ray band, is produced by the same particles that are responsible for the production of the Compton high energy tail at $E_\gamma > 1$ GeV, which is too weak to be detected during the low state (when the observed X–rays are dominated by the Compton component).

4.4. Comparison of AO 0235+164 to X–ray Selected BL Lac Objects

It is interesting to compare the X–ray and γ–ray properties of classical, radio-selected BL Lac objects to these selected or classified on the basis of their X–ray emission (for the discussion of the two sub-classes of

BL Lacs, see, e.g., Stocke et al. 1989; Giommi et al. 1990). In general, relatively few BL Lacs as compared to OVV quasars have been detected in the GeV energies. Admittedly, selection criteria are not very rigorous, but, while the X–ray surveys continue to reveal new objects, the detection of GeV γ–rays in X–ray selected BL Lacs is restricted to two objects. One is Mkn 421, which shows consistently only a modest GeV flux, despite the relative proximity (see Lin et al. 1992; Fichtel et al. 1994). The other is PKS 2155-304, only recently detected by Egret at a fairly faint level (Vestrand et al. 1995). It is interesting to compare the 1 GeV – to 1 keV flux ratios of X–ray selected BL Lac objects from the Piccinotti survey (Mkn 421, PKS 0548-322, PKS 2155-304, Mkn 501, and 1218+304) to that measured by us for AO 0235+164. Both PKS 2155-304 (Vestrand et al. 1995) and Mkn 421 (Lin et al. 1992) are detected at a faint level; the remaining three have published GeV upper limits (Fichtel et al. 1994). We list these, together with 1 keV flux densities in Table 3. To arrive at the 1 GeV flux upper limits, we use the same conversion of the photon count rate to 1 GeV flux density as for AO 0235+164 (which, with an assumed $\alpha = 1$, is 1×10^{-7} photons (> 100 MeV) cm^{-2} s^{-1} = 1.6×10^{12} Jy$\times$Hz).

It is apparent from Table 3 that the ratio of the observed 1 GeV flux densities (or upper limits) to these measured at 1 keV is substantially lower in the X–ray selected BL Lac objects than we observe in AO 0235+164. We acknowledge that the X–ray data for these objects are not simultaneous with the GeV observations, but, given the multiple Egret pointings at the regions of the sky where these objects are located, the difference is likely real. This difference may be explained by the recent finding by Padovani and Giommi (1995), who note that the peak of the overall radio – through – X–ray flux distribution (in $E \times F(E)$) in X–ray selected BL Lacs is shifted towards higher frequencies, $\sim 10^{15} - 10^{16}$ Hz, as compared to $\sim 10^{13} - 10^{14}$ Hz for the radio-selected objects. In this scenario, in the X–ray selected objects the tail of the synchrotron emission dominates the soft X–ray spectrum, and makes the contribution of the Compton radiation – if present at all – undetectable, in contrast to the radio selected BL Lacs, as AO 0235+164, where emission due to *both* processes has been observed. If this is the case, a more meaningful comparison would be the ratio of the *peak of the synchrotron emission to the peak of the γ–ray emission.* In any case, there appears to be a clear conclusion – *selecting BL Lac objects via X–ray techniques does not lead to selection of the brightest γ–ray emitting BL Lacs.*

5. Conclusions

We observed the BL Lac object AO 0235+164 with ROSAT, and then 6 moths later simultaneously with Asca and CGRO Egret. Our observations revealed the following :

(1) ROSAT data show that AO 0235+164 is rapidly variable in X–rays, with a rapid (< 4 days) rise, and a more gradual decay. No variability is observed in the Asca or Egret data.

(2) The comparison of ROSAT and Asca observations shows strong spectral variability in X–rays, with a change of the energy power law index from ~ 2 in ROSAT data to ~ 1 in Asca data (when the source was fainter). We interpret this as a signature of the steep tail of the electron distribution radiating via synchrotron emission dominating the higher flux ROSAT observation, and the fainter, harder Compton emission dominating the Asca observation.

(3) The excess absorption reported on the basis on the Einstein IPC data in this object is real, but it is currently less that the 1980 IPC data imply. Due to the instrumental uncertainties of the Einstein IPC, we consider the variability of the absorbing column as only tentative. The ROSAT PSPC and Asca data are in close agreement with each other on the column density of the absorber; under an assumption that it is at $z = 0$, it is $\sim 2.2 \times 10^{21}$ cm^{-2} equivalent H atoms above the Galactic value. The statistical quality of the X–ray data does not allow us to determine the location of the absorber; independently, the IRAS 100 μm data support the hypothesis that the excess absorption is not in our Galaxy. Given

the IUE observations of Snijders et al. (1982), we conclude that this absorber is due to the intervening galaxy at the redshift of 0.524, and is the same material which is observed in the optical and radio, with a corresponding X–ray column of the Morrison & McCammon (1983) absorber (i.e. at the Solar ratio of elements) of 4.2×10^{21} equivalent H atoms cm^{-2}.

(4) Even in the unlikely case if all the absorption observed by us in the $z = 0.524$ system is due to primordial helium, the comparison of the X–ray absorption to the 21 cm radio absorption limits the hydrogen spin temperature T_S to less than 700 K. The knowledge of T_S via independent means will enable a measurement of the abundances A of chemically processed elements in this system (as compared to hydrogen, and as a fraction of the Solar value); assuming the ratio of chemically processed elements to each other to be Solar, at $T_S = 460$ K, A is $\sim 0.14 \pm 0.11$; at $T_S = 140$ K, A is $\sim 1.3 \pm 0.3$.

(5) Simultaneous Asca – Egret observation of AO 0235+164 shows that the $E \times F(E)$ at 1 GeV is about 30 times the X–ray (1 keV) $E \times F(E)$; this value is nearly 4 times greater than the ratio of GeV to X–rays for 3C279 in the low state. This factor of 30 is also *very* substantially greater than for X–ray selected BL Lac objects, where, for instance, a value of 0.6 is inferred for PKS 2155-304, suggesting important differences in the structure or orientation of the beamed emission between the two sub-classes of BL Lacs.

Acknowledgements: We are grateful to Dr. Steve Snowden for the help with the access and interpretation of the IRAS data, Prof. John Stocke for discussions on taxonomy of BL Lac objects, Prof. John Bally and Dr. Richard Mushotzky for discussions on the nature of the intervening absorber, the referee, Prof. Thierry Courvoisier, for suggestions resulting in a clarification of some points in the paper, and Prof. Mitch Begelman for many useful comments on the manuscript and hospitality at the Univ. of Colorado. This research was supported by the Grants-in Aid by the Ministry of Education, Culture, and Science (Monbusho) of Japan (05242101), and by NASA, via GRO grant NAG5-2439, and ROSAT and Asca observing grants.

REFERENCES

Abraham, R.G., Crawford, C.S., Merrifield, M., Hutchings, J.B., and McHardy, I. 1993, ApJ, 415, 101.

Bania, T.M., Marscher, A.P., and Barvainis, R. 1991, AJ, 101, 2147.

Blandford, R.D., and Königl, 1979, 232, 34.

Boulanger, F., and Perault, M. 1988, ApJ, 330, 964.

Bregman, J., et al. 1984, ApJ, 276, 454.

Briggs, F.H., and Wolfe, A.M. 1983, ApJ, 268, 76.

Brinkman, W., et al. 1994, A&A, 288, 433.

Burbidge, E.M., Caldwell, R.D., Smith, H.E., Liebert, J., and Spinrad, H. 1976, ApJ, 205, L117.

Cohen, R.D., Smith, H.E., Junkkarinen, V.T., and Burbidge, E.M. 1987, ApJ, 318, 577.

Dame, T.M., et al. 1987, ApJ, 322, 706.

Dermer, C., Schlickheiser, R., and Mastichiadis, A. 1992, A&A, 256, L27

Edelson, R., et al. 1995, ApJ, 438, 120.

Elvis, M., Lockman, F.J., and Wilkes, B. 1989, AJ, 97, 777.

Fichtel, C.E., et al. 1994, ApJS, 94, 551.

Ghisellini, G., and Maraschi, L., 1989, ApJ, 340, 181

Giommi, P., Barr, P., Garilli, B., Maccagni, D., and Pollock, A.M.T. 1990, ApJ, 356, 432.

Hartman, R., et al. 1992, ApJ, 385, L1.

Hunter, S., et al. 1993, A&A, 272, 59.

Kii, T., et al. 1992, in Frontiers of X–Ray Astronomy, ed. Y. Tanaka and K. Koyama (Tokyo: Universal Academy Press), 577.

Kniffen, D.A., et al. 1993, ApJ, 411, 133.
Königl, A. 1981, ApJ, 243, 700.
Lin, Y.C., et al. 1992, ApJ, 401, L61.
Madejski, G.M. 1985, PhD Thesis, Harvard University.
Madejski, G.M., and Schwartz, D.A. 1988, ApJ, 330, 776.
Madejski, G.M., Mushotzky, R.F., Weaver, K.A., Arnaud, K.A., and Urry, C.M. 1991, Ap. J., 370, 198.
Madejski, G.M. 1994, ApJ 432, 554.
Maraschi, L., Ghisellini, G., and Celotti A. 1992, ApJ, 397, L5.
Maraschi, L., et al. 1994, ApJ, 435, L91.
Marscher, A.P., and Gear, W.K. 1985, ApJ, 298, 114.
Marscher, A. 1988a, ApJ, 334, 552.
Marscher, A. 1988b, in "The Impact of VLBI on Astrophysics and Geophysics" (Dordrecht: Reidel), eds M.J. Reid and J.M. Moran, 35.
Mattox, J.R., et al. 1993, ApJ, 410, 609.
von Montigny, C., et al. 1995, ApJ, 440, 525.
Morrison, R., and McCammon, D. 1983, ApJ, 270, 119.
Olive, K.A., and Steigman, G. 1995, ApJS, 97, 49.
Ostriker, J.P., and Vietri, M. 1985, Nature, 318, 446.
Padovani, P., and Giommi, P. 1995, ApJ, 444, 567.
Rees, M.J. 1967, MNRAS, 137, 429.
Rieke, G.H., Grasdalen, G.L., Kinman, T.D., Hintzen, P., Wills, B.J., and Wills, D. 1976, Nature, 260, 754.
Roberts, M.S., Brown, R.L., Brundage, W.D., Rots, A.H., Haynes, M.P., and Wolfe, A.M. 1976, AJ, 81, 293.
Sambruna, R., Barr, P., Giommi, P., Maraschi, L., Tagliaferri, G., and Treves, A. 1994, ApJ, 434, 468.
Sembay, S., et al. 1993, ApJ, 404, 112.
Sikora, M., Begelman, M., and Rees, M. 1994, ApJ, 421, 153.
Snijders, M.A.J., Boksenberg, A., Penston, M.V., & Sargent, W.L.W. 1982, MNRAS, 201, 801.
Spinrad, H., and Smith, H. 1975, ApJ, 201, 275.
Stocke, J.T., Morris, S.M., Gioia, I.M., Maccacaro, T., Schild, R.E., and Wolter, A. 1989, in BL Lac Objects (Springer-Verlag: Berlin), eds. L. Maraschi, T. Maccacaro, and M.-H. Ulrich, 242.
Tashiro, M. 1992, Ph.D. Thesis, University of Tokyo.
Tashiro, M., Makishima, K., Ohashi, T., Inda-Koide, M., Yamashita, A., Mihara, T., & Kohmura, Y. 1995, PASJ, 47 (2), 131.
Turner, T.J., George, I.M., Madejski, G.M., Kitamoto, S., and Suzuki, T. 1995, ApJ, 445, 660.
Vestrand, W.T., Stacy, J.G., and Sreekumar, P. 1995, IAU Circular 6169.
Wheelock et al. 1994, IRAS Sky Survey Atlas, JPL Publication 94-11 (Pasadena: JPL).
Wolfe, A.M., and Wills, B. 1977, ApJ, 218, 39.
Wolfe, A.M., Davis, M.M., and Briggs, F.H. 1982, ApJ, 259, 495.

FIGURE CAPTIONS

Fig. 1: The light curve (a, top panel) and softness ratio (b, bottom panel) for the ROSAT observations of AO 0235+164, clearly showing the flux variability.

Fig. 2: The data (top panel) and residuals (bottom panel) for the summed ROSAT observation of AO 0235+164, fitted to a power law model, absorbed by a gas with abundances and cross-sections given by Morrison & McCammon, located at $z = 0$.

Fig. 3: The data (top panel) and residuals (bottom panel) for the summed GIS2 data for the Asca observation of AO 0235+164, fitted to a power law model, absorbed by a gas with abundances and cross-sections given by Morrison & McCammon, located at $z = 0$.

Fig. 4: Confidence contours ($\chi^2 + 2.3, 4.6$, and 9.2) on the absorbing column density (at $z = 0$) and power law index for ROSAT data (upper contours) and Asca data (lower contours). The comparison of the two data sets clearly indicates index variability, but no absorption variability. The absorption is clearly in excess of the Galactic value of 7.6×10^{20} cm^{-2}.

Fig. 5: $\Delta\chi^2$ (as compared to the best fit) plotted against the equivalent hydrogen column density of Morrison - McCammon absorber (at $z = 0.524$) (beyond the fixed Galactic absorption at 7.6×10^{20} cm^{-2}) in the combined ROSAT and Asca data. The fit required that the absorption is the same between Asca and ROSAT, but allowed for the power law index and normalization to vary independently.

Fig. 6a: Confidence regions ($\chi^2_{min} + 2.3, 4.6$, and 9.2) on the "primordial" absorber (with the primordial H to ^{4}He ratio) plotted against the "chemically processed" absorber (where the elemental abundances are Solar *minus* the "primordial"). It is clear that the true hydrogen column density $N_{\rm H}$ cannot exceed 1.6×10^{22} cm^{-2}, as any admixture of reprocessed material would only reduce the absorbing column. This plus the redshifted 21 cm data of Roberts et al. (1976) yield the plotted upper limit on the spin temperature $T_{\rm S} < 700$K. Two vertical lines mark the column densities for $T_{\rm S} = 460$ K (implying metallicity A of 0.14 ± 0.11 Solar) and $T_{\rm S} = 140$ K (implying metallicity A of 1.3 ± 0.3 Solar). **Fig. 6b:** As in Figure 6a, but the vertical axis is the equivalent hydrogen column density of material consisting entirely of oxygen. The X–ray data allow up to $\sim 7 \times 10^{18}$ cm^{-2} of absorbing column of pure oxygen, and are consistent with material entirely devoid of oxygen.

Fig. 7: Simultaneous X–ray – to γ–ray $E \times F(E)$ spectrum of AO 0235+164 obtained in February 1994. The X–ray data are plotted as observed, i.e. including the effects of absorption. Note that the source was detected in each of the plotted Egret spectral bands only at 2 to 3 σ, but the plot is meant to illustrate that the source spectrum is consistent with a power law model with $\alpha = 1$, previously reported by Hunter et al. (1993).

Table 1. Summary of the ROSAT and Asca observations of AO 0235+164

Exposure name (a)	Observation start time (UT) (b)	"On-source" time (c)	Net source counting rate (d)	Background counting rate (in a det. cell) (e)	Net soft/hard count rate ratio (ct rt<1 keV/ct rt>1 keV) (f)
A. ROSAT PSPC data					
R1	07/21/93 05:32	2083	0.201 +/- 0.010	0.0069	0.81 +/- 0.083
R2	07/24/93 02:00	1903	0.359 +/- 0.014	0.0074	0.96 +/- 0.075
R3	07/26/93 19:18	1508	0.287 +/- 0.014	0.0102	0.88 +/- 0.087
R4	07/29/93 14:14	1192	0.175 +/- 0.013	0.0108	0.90 +/- 0.133
R5	08/01/93 09:12	1783	0.143 +/- 0.010	0.0084	1.02 +/- 0.134
R6	08/04/93 08:52	2023	0.118 +/- 0.008	0.0143	0.93 +/- 0.132
R7	08/06/93 21:56	4099	0.101 +/- 0.005	0.0086	0.98 +/- 0.102
R8	08/12/93 11:42	1664	0.093 +/- 0.008	0.0068	0.94 +/- 0.163
R9	08/15/93 08:10	1708	0.077 +/- 0.007	0.0055	0.72 +/- 0.141
Total ROSAT		17963	0.166 +/- 0.0032		
B. Asca data					
A1: GIS2	02/04/94 19:33	11858	0.021 +/- 0.0026		
GIS3		11858	0.029 +/- 0.0028		
SIS0		11164	0.038 +/- 0.0052		
SIS1		10664	0.032 +/- 0.0055		
A2: GIS2	02/11/94 22:36	12383	0.023 +/- 0.0027		
GIS3		12334	0.028 +/- 0.0026		
SIS0		10930	0.041 +/- 0.0053		
SIS1		10406	0.032 +/- 0.0056		
A3: GIS2	02/16/94 01:25	11592	0.018 +/- 0.0027		
GIS3		11592	0.028 +/- 0.0028		
SIS0		10189	0.037 +/- 0.0056		
SIS1		9939	0.028 +/- 0.0058		
A4: GIS2	02/19/94 03:55	12399	0.023 +/- 0.0026		
GIS3		12397	0.030 +/- 0.0027		
SIS0		12146	0.041 +/- 0.0048		
SIS1		11725	0.038 +/- 0.0050		
Total Asca	GIS2	48232	0.0214 +/- 0.0009		
	GIS3	48181	0.0286 +/- 0.0010		
	SIS0	44429	0.0385 +/- 0.0016		
	SIS1	42734	0.0322 +/- 0.0016		

Table 2. Spectral fits to the Asca and ROSAT data for AO 0235+164

	Model :				
	Power law plus free absorption at z=0		**Power law plus Galactic absorption at z = 0 plus free absorption at z = 0.524**		
Data set	**Power law energy index**	**Absorption (x10^21 cm^-2)**	**Power law energy index**	**Gal. abs. (x10^21 cm^-2) (fixed)**	**z = 0.524 absorption (x10^21 cm^-2)**
(a)	**(b)**	**(c)**	**(d)**	**(e)**	**(f)**
Data sets fitted separately					
ROSAT	2.03 (+0.50, -0.45)	3.0 (+0.8, -0.7)	1.67 (+0.32, -0.32)	0.76	3.8 (+1.2, -1.1)
chi sq. / # PHA ch.	30.2 / 40		27.4/40		
Asca 0.5 - 10 keV	1.01 (+0.09, -0.10)	2.75 (+0.51, -0.47)	0.96 (+0.09, -0.09)	0.76	4.6 (+1.3, -1.3)
chi sq. / # PHA ch.	341 / 354		340 / 354		
Asca 0.5 - 2 keV	0.72 (+0.42, -0.43)	2.2 (+0.9, -1.0)	0.61 (+0.30, -0.31)	0.76	2.8 (+1.9, -1.6)
chi sq. / # PHA ch.	155 / 165		151 / 165		
Data sets fitted together*					
ROSAT	1.92 (+0.25, -0.27)	2.82 (+0.40, -0.41)	1.77 (+0.25, -0.23)	0.76	4.15 (+0.92, -0.84)
Asca	1.02 (+0.08, -0.08)	2.82 (+0.40, -0.41)	0.93 (+0.08, -0.07)	0.76	4.15 (+0.92, -0.84)
chi sq. / # PHA ch.	371 / 394		368 / 394		

Notes :

*The joint fit assumed that the absorption between the ROSAT and Asca data sets are the same, but the power law index was allowed to vary between the two data sets. Note that this is equivalent to a "soft excess" model parametrized as a broken power law, with the energy of the break varying from the ROSAT to the Asca observation epochs.

All errors are 90 % confidence regions (chi sq. + 2.7)

Table 3. Comparison of the ratio of 1 GeV - to 1 keV fluxes for AO 0235+164 and X-ray selected BL Lac objects

Object name	Flux density in microJansky			Average 1 keV flux density (Jy*Hz)	Egret > 100 MeV photon flux (x 10e-7 ph/cm^2/s)	1 GeV flux density (Jy*Hz)	1 GeV / 1 keV flux ratio
	Einstein*	EXOSAT*	Asca				
(a)	(b)	(c)	(d)	(e)	(f)	(g)	(h)
AO 0235+164			0.3	7.44E+10	1.4	2.2E+12	30
X-ray selected BL Lac objects							
PKS 0548-322	9.0	5.9		1.79E+12	< 0.8	< 1.3E+12	< 0.70
1218+304	4.4	8.5		1.55E+12	< 0.6	< 9.4E+11	< 0.6
Mkn 501	23.7	13.8		4.50E+12	< 0.8	< 1.3E+12	< 0.28
Mkn 421	2.0	13.8		1.90E+12	2.1	3.3E+12	1.7
PKS 2155-304	29.0	28.5		6.90E+12	2.7	4.2E+12	0.61

Notes : * Einstein fluxes from Madejski et al. (1991); EXOSAT fluxes from Sambruna et al. (1994);
Egret flux for PKS 2155-304 from Vestrand et al. (1995); other Egret fluxes and
upper limits for the X-ray selected objects from Fichtel et al (1994).
The data for the X-ray selected objects are not simultaneous with the Egret data.

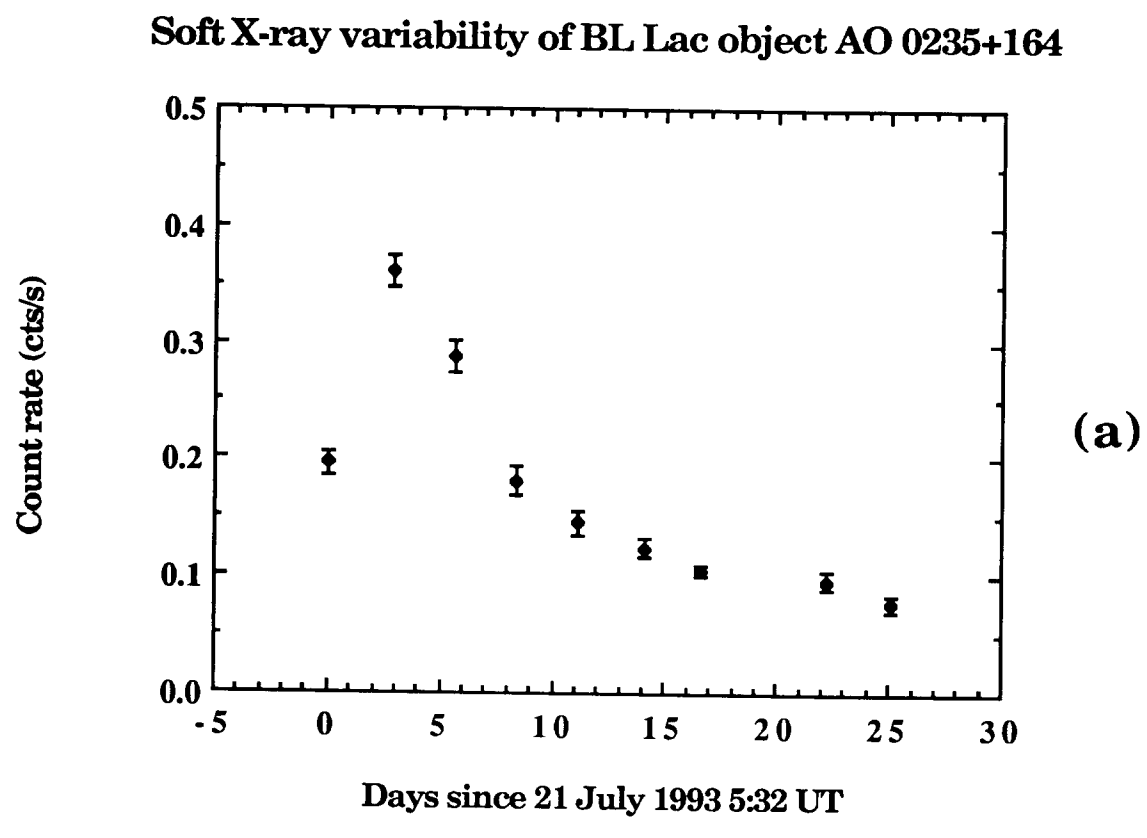
Soft X-ray variability of BL Lac object AO 0235+164
Count rate (cts/s)
0.5
0.4
0.3
0.2
0.1
0.0
-5
0
5
10
15
20
25
30
Days since 21 July 1993 5:32 UT
(a)
ROSAT softness ratio for AO 0235+164
softness ratio (<1 keV / >1 keV)
1.2
1.0
0.8
0.6
0.4
-5
0
5
10
15
20
25
30
Days since 21-jul-93 5:32 UT
(b)

Figure 1

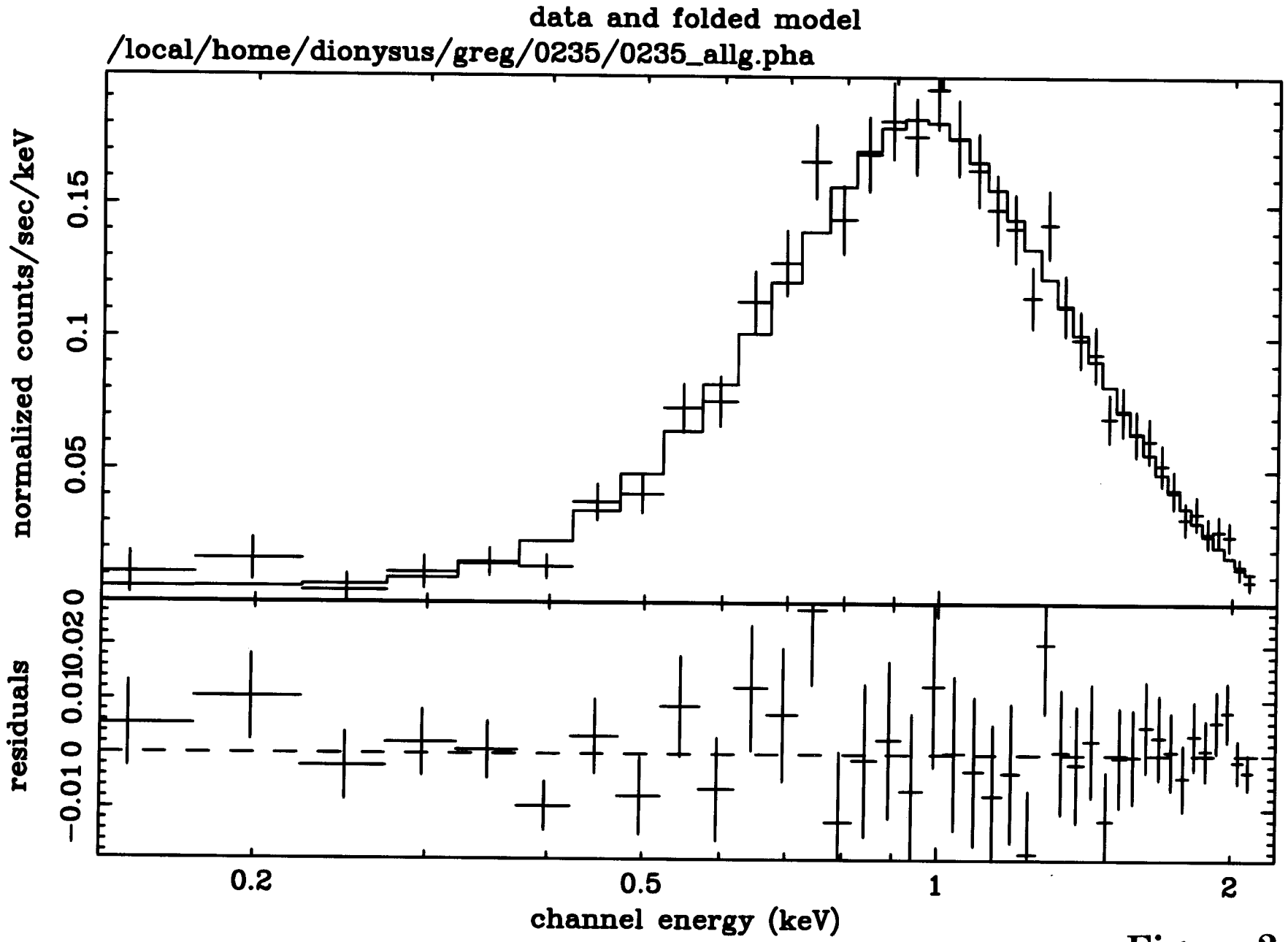
data and folded model
/local/home/dionysus/greg/0235/0235_allg.pha
normalized counts/sec/keV
0.15
0.1
0.05
0
residuals
0.02
0.01
0
−0.01
0.2
0.5
1
2
channel energy (keV)

Figure 2

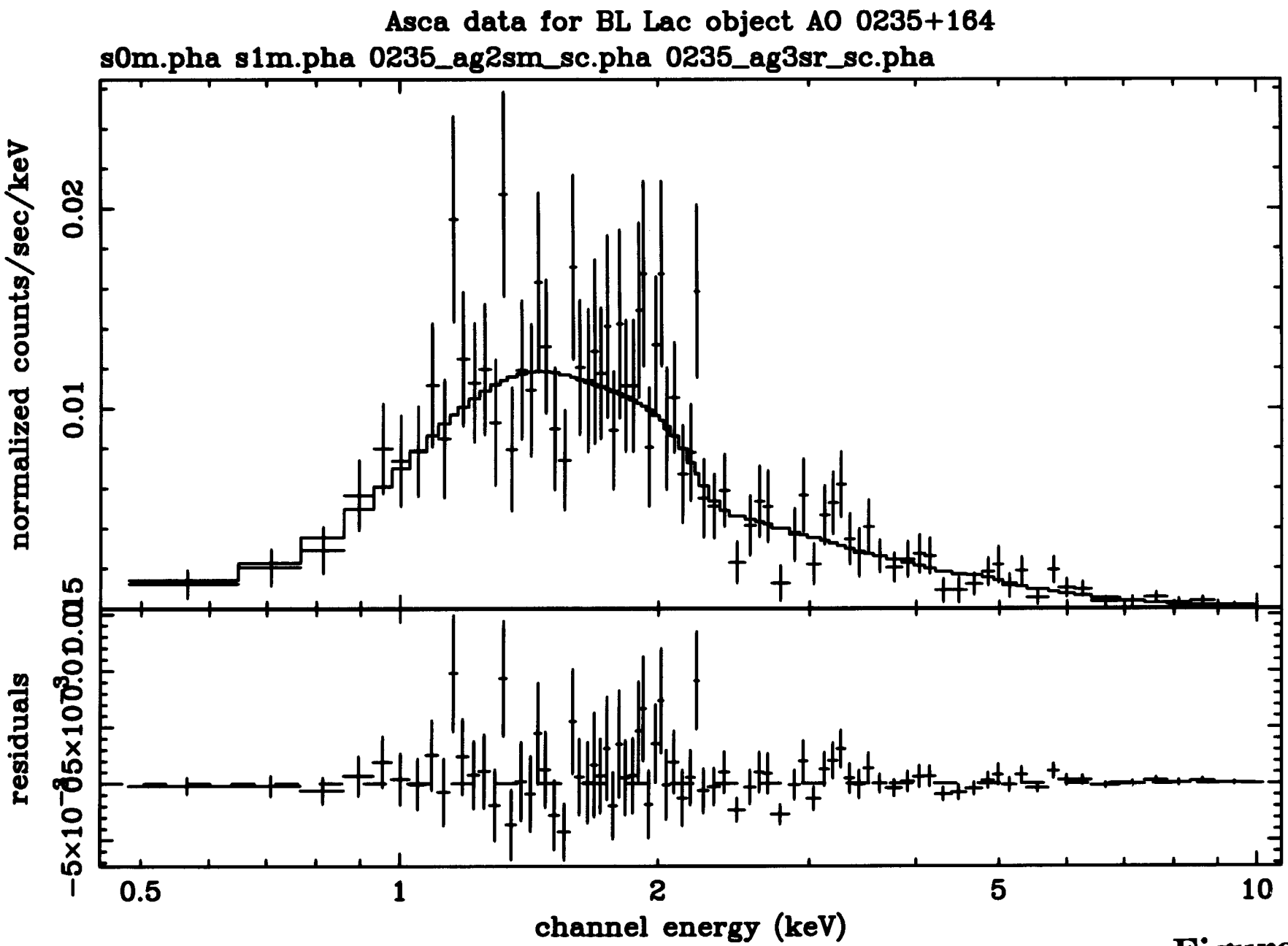
Asca data for BL Lac object A0 0235+164
s0m.pha s1m.pha 0235_ag2sm_sc.pha 0235_ag3sr_sc.pha
normalized counts/sec/keV
0.02
0.01
residuals
0.005
0
−5×10⁻³
0.5
1
2
5
10
channel energy (keV)

Figure 3

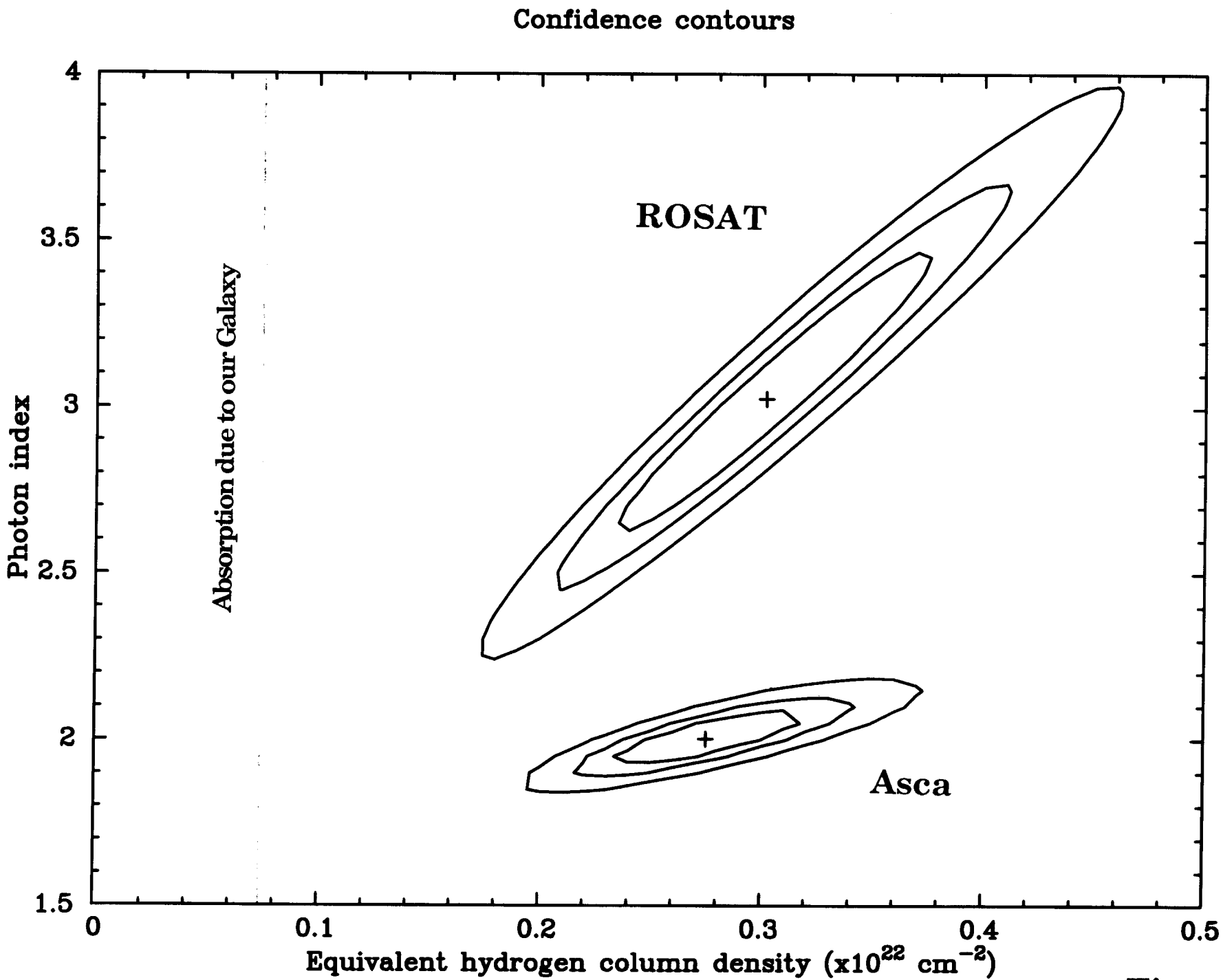
Confidence contours
ROSAT
Asca
Photon index
Absorption due to our Galaxy
Equivalent hydrogen column density (x10^22 cm^-2)
4
3.5
3
2.5
2
1.5
0
0.1
0.2
0.3
0.4
0.5

Figure 4

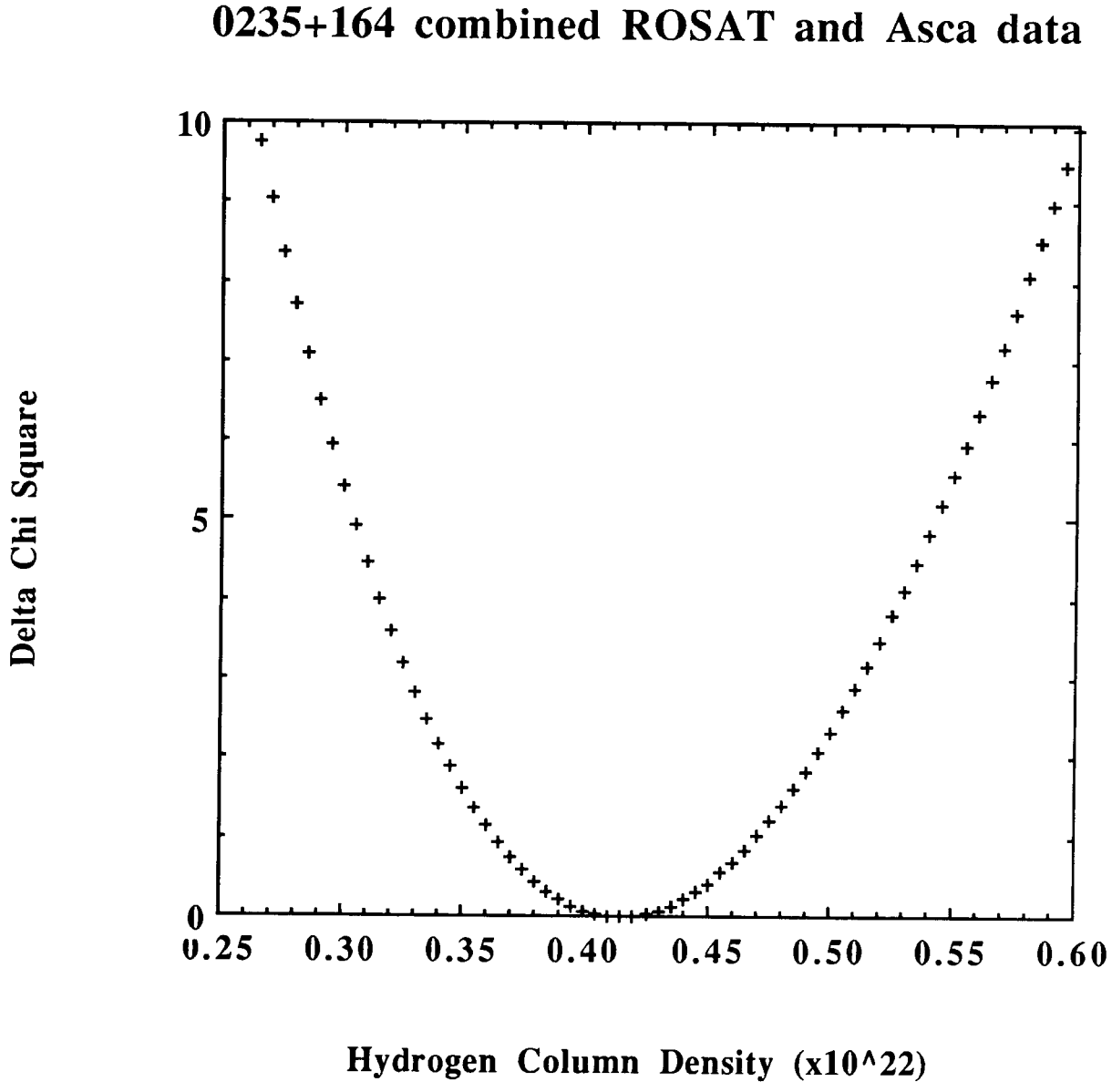
0235+164 combined ROSAT and Asca data
Delta Chi Square
10
5
0
0.25
0.30
0.35
0.40
0.45
0.50
0.55
0.60
Hydrogen Column Density (x10^22)

Figure 5

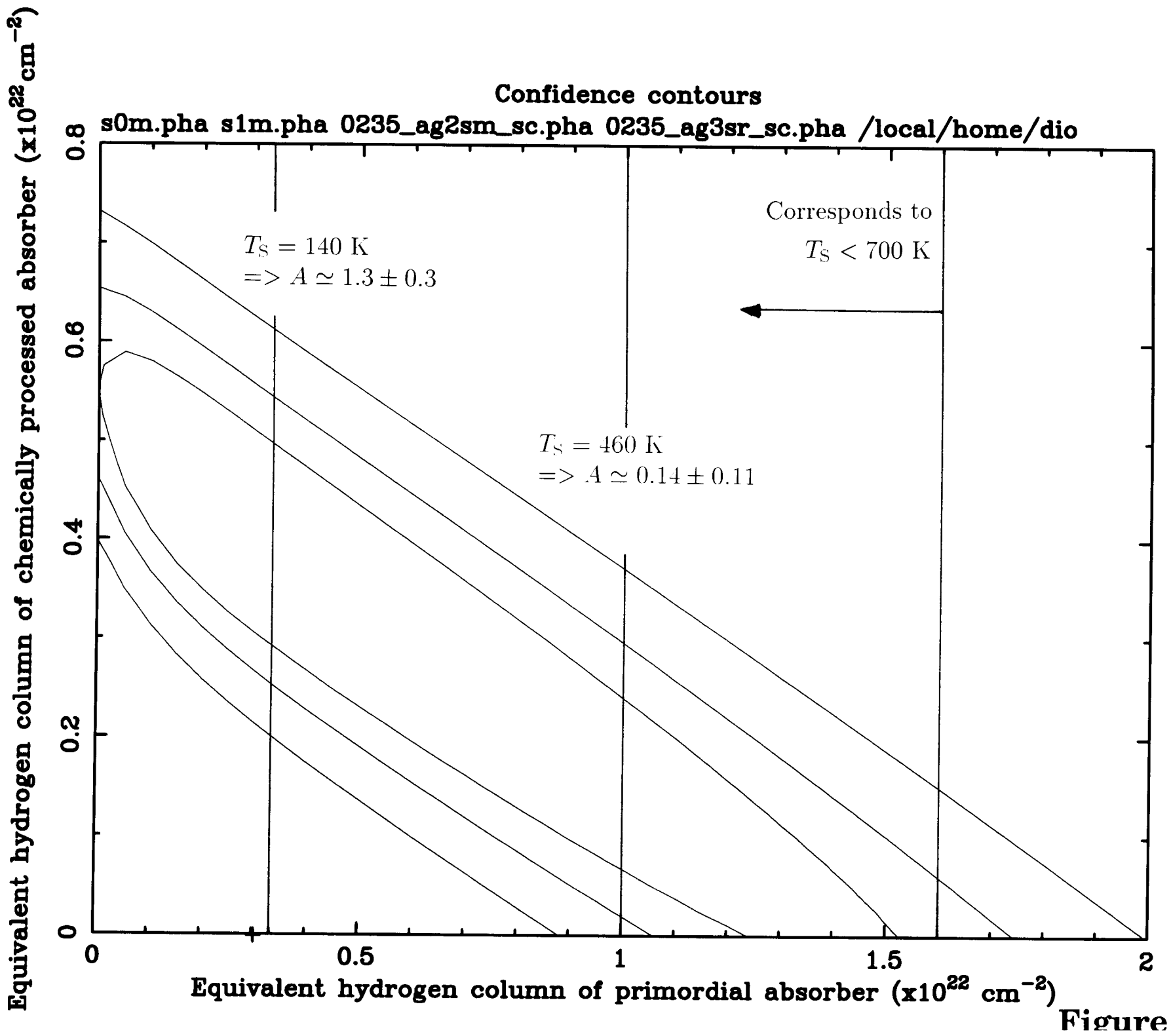
Confidence contours
s0m.pha s1m.pha 0235_ag2sm_sc.pha 0235_ag3sr_sc.pha /local/home/dio
Corresponds to
$T_S < 700$ K
$T_S = 140$ K
=> $A \simeq 1.3 \pm 0.3$
$T_S = 460$ K
=> $A \simeq 0.14 \pm 0.11$
Equivalent hydrogen column of chemically processed absorber (x10^{22}cm^{-2})
Equivalent hydrogen column of primordial absorber (x10^{22} cm^{-2})
0
0.2
0.4
0.6
0.8
0.5
1
1.5
2

Figure 6 (a)

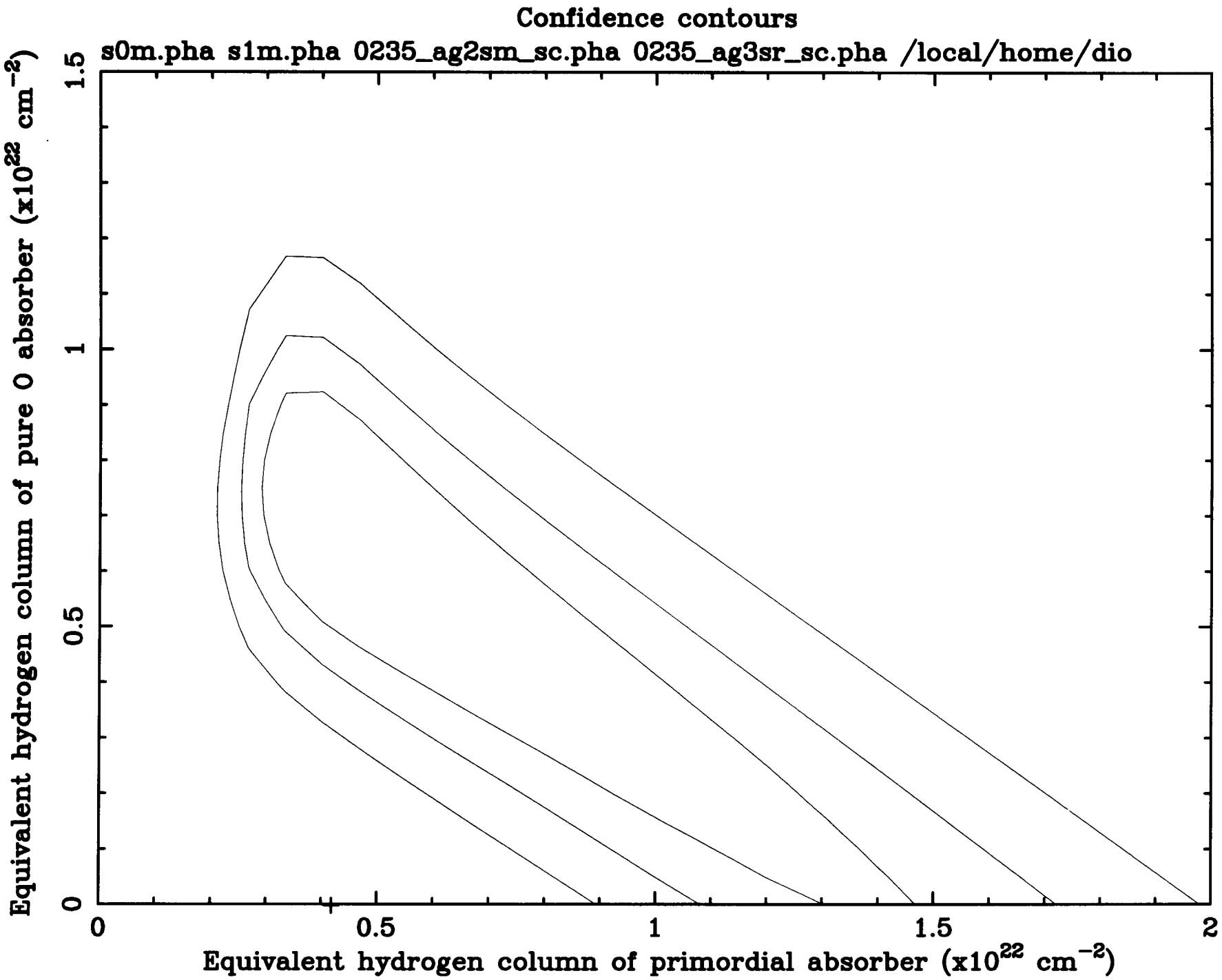
Confidence contours
s0m.pha s1m.pha 0235_ag2sm_sc.pha 0235_ag3sr_sc.pha /local/home/dio
Equivalent hydrogen column of pure O absorber (x10^22 cm^-2)
0
0.5
1
1.5
0
0.5
1
1.5
2
Equivalent hydrogen column of primordial absorber (x10^22 cm^-2)

Figure 6 (b)

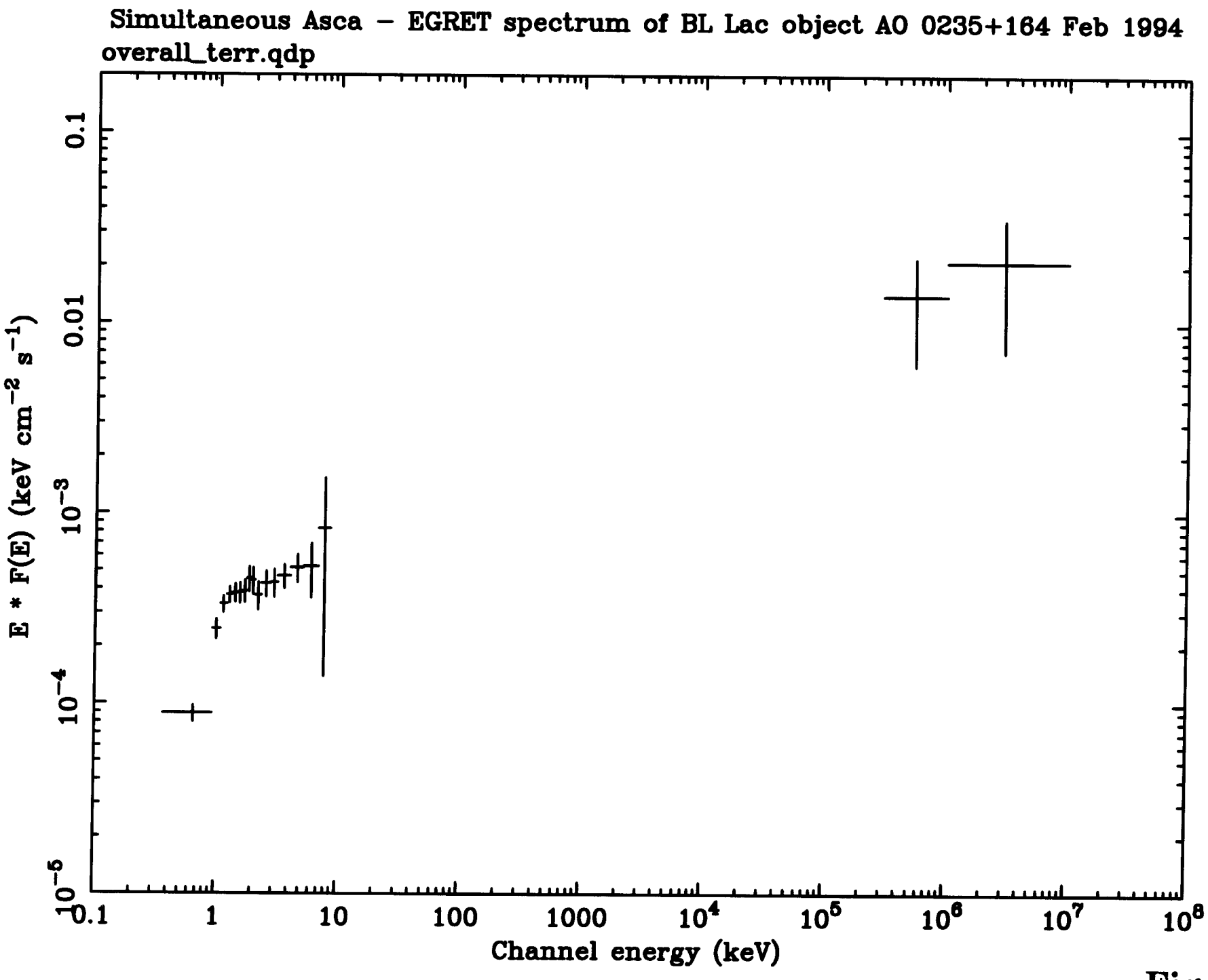
Simultaneous Asca – EGRET spectrum of BL Lac object A0 0235+164 Feb 1994
overall_terr.qdp
E * F(E) (keV cm^{-2} s^{-1})
0.1
0.01
10^{-3}
10^{-4}
10^{-5}
0.1
1
10
100
1000
10^4
10^5
10^6
10^7
10^8
Channel energy (keV)

Figure 7